NIH Public Access
Author Manuscript
Cytometry A. Author manuscript; available in PMC 2011 December 1.

Published in final edited form as:
Cytometry A. 2010 December ; 77(12): 1113–1125. doi:10.1002/cyto.a.20964.

Time-resolved microscopy for imaging lanthanide luminescence in living cells

Nivriti Gahlaut and **Lawrence W. Miller***
Department of Chemistry, University of Illinois at Chicago, Chicago, USA

Abstract

Time-resolved luminescence (TRL) microscopy can image signals from lanthanide coordination complexes or other probes with long emission lifetimes, thereby eliminating short-lifetime (< 100 ns) autofluorescence background from biological specimens. However, lanthanide complexes emit far fewer photons per unit time than conventional fluorescent probes, making it difficult to rapidly acquire high quality images at probe concentrations that are relevant to live cell experiments. This article describes the development and characterization of a TRL microscope that employs a light-emitting diode (LED, λ_{em} = 365 nm) for pulsed epi-illumination and an intensified charge-coupled device (ICCD) camera for gated, widefield detection. Europium chelate-impregnated microspheres were used to evaluate instrument performance in terms of short-lifetime fluorescence background rejection, photon collection efficiency, image contrast and signal-to-noise ratio (SNR). 200 nm microspheres were imaged within the time resolution limit of the ICCD (66.7 ms) with complete autofluorescence suppression. 40 nm microspheres containing ~400 chelate molecules were detected within ~1 s acquisition times. A luminescent terbium complex, Lumi4-Tb®, was introduced into the cytoplasm of cultured cells at an estimated concentration of 300 nM by the method of osmotic lysis of pinocytic vesicles. Time-resolved images of the living, terbium complex-loaded cells were acquired within acquisition times as short as 333 ms, and the effects of increased exposure time and frame summing on image contrast and SNR were evaluated. The performance analyses show that TRL microscopy is sufficiently sensitive and precise to allow high-resolution, quantitative imaging of lanthanide luminescence in living cells under physiologically relevant experimental conditions.

Key Terms

Fluorescence Microscopy; Lanthanide; Time-Resolved; Signal-to-Noise Ratio

Introduction

The sensitivity and precision of fluorescence-based bioassays and microscopy is often diminished by autofluorescence background emitted from samples and containers or coverslips. Time-resolved luminescence (TRL) measurements can effectively eliminate autofluorescence when the detected analyte has an emission lifetime exceeding that of endogenous fluorophores (< 100 ns).(1) TRL instrumentation uses a finite pulse of light to excite a sample (Fig. 1). Then, the detector is electronically switched on, or unshuttered after a short interval (the gate delay) during which sample autofluorescence has diminished. The detector remains on for a finite interval (the gate width), and the output from multiple excitation/emission cycles can be integrated to increase signal.

*Correspondence to: Lawrence W. Miller; Department of Chemistry, 845 W. Taylor Street, Chicago, IL, 60607, Ph: 312 996 8542, Fax: 312 996 0431, lwm2006@uic.edu.

NIH-PA Author Manuscript
NIH-PA Author Manuscript
NIH-PA Author Manuscript

NIH-PA Author Manuscript

NIH-PA Author Manuscript

NIH-PA Author Manuscript

The most common emissive probes for TRL-based bioassays are ligand-sensitized, coordination complexes of lanthanide cations. Lanthanide complexes (LCs) have long lifetimes (μs – ms) that facilitate TRL detection as well as large Stokes shifts (> 150 nm) and multiple, narrow emission bands that make it easy to spectrally isolate signals.(2–4) Because lanthanide absorption transitions are parity-forbidden, direct excitation is inefficient, and LCs typically incorporate an organic chromophore that absorbs light and indirectly excites the chelated metal via intramolecular energy transfer. Considerable effort has been devoted to developing luminescent LCs that are kinetically and thermodynamically stable, water soluble and easily conjugated to biomolecules, and some terbium and europium LCs have high extinction coefficients (>10,000 M^{-1} cm^{-1}) and quantum yields up to 1.0 in aqueous solution.(5–9) TRL detection of resonance energy transfer between LC donors and short-lifetime organic or protein fluorophore acceptors has been exploited extensively for high-throughput, cell-free assays of biomolecular interactions, and picomolar detection limits of LC-labeled analytes have been achieved.(4,10–13) Other long-lived probes have also been developed for TRL applications, including metal-ligand complexes of platinum and palladium that emit with shorter lifetimes than LCs (100 ns – 10 μs) and that can be excited with visible light.(14–16)

Continued advancement in luminescent probe development, and the clear enhancements in sensitivity achievable with TRL detection have led a number of investigators to develop TRL microscopes.(17) Early TRL microscopes used mechanical choppers to modulate continuous wave excitation sources and effectively shutter CCD cameras.(18–22) Later iterations employed electronically gated sources and/or detectors to achieve synchronized excitation and emission.(8,10,14,17,23–29) Excitation of terbium or europium LCs requires near-UV radiation, and pulsed xenon flashlamps,(8,18–19,22,24,28) nitrogen lasers,(10) Nd-YAG lasers,(23) He-Cd lasers,(27) and UV light emitting diodes (LED's)(17,30–32) have all been employed as sources. Intensified CCD (ICCD) cameras offer an effective means of shuttering emission light, as the image intensifier can be gated on/off with nanosecond resolution while simultaneously amplifying the emission signal, and the latest ICCD cameras offer good quantum efficiency (~50%) and small effective pixel sizes (~10 μm). Direct gating of interline transfer CCD detectors(33–34) and electron multiplying CCD's(17,30) for TRL imaging applications has also been reported. While most of the reported TRL microscopes comprised modifications of epi-fluorescence systems, Saavedra and co-workers developed a time-resolved total internal reflection microscope.(27) Time-resolved, multiphoton scanning microscopy based on shifting the detection pinhole to collect delayed luminescence from a position lagging the rasting laser beam was recently reported by Ramshesh and Lemasters.(35)

Recently, investigators have begun to explore the potential benefits of long-lifetime probes for cellular imaging applications.(2,6,8,14,36–38) LCs have been imaged within living cells using TRL microscopy with pulsed, near-UV single photon or two photon excitation, (8,24,26,36) and live-cell TRL microscopy in the microsecond domain has been demonstrated using platinum complexes.(14) While these early studies showcased the ability to discriminate probe emission from autofluorescence background, the potential disadvantages of reduced signal have not been addressed. The signal-to-noise ratio (SNR) is one measure of microscope image quality, and SNR cannot exceed the square root of the number of photons/pixel.(39) As the rate of photon emission from a single molecule is inversely proportional to its lifetime,(1) LCs or other long-lifetime probes may be expected to emit orders of magnitude fewer photons per unit time than conventional fluorophores such as green fluorescent protein or fluorescein that emit with nanosecond-scale lifetimes. Therefore, despite autofluorescence background reduction, the SNR achievable with TRL microscopy may be substantially lower than that observed with conventional, steady-state

NIH-PA Author Manuscript

NIH-PA Author Manuscript

NIH-PA Author Manuscript

fluorescence microscopy under conditions of probe concentration and image acquisition time that are relevant to live cell imaging.

We report here the development and characterization of a TRL microscope employing epi-illumination and wide-field detection. The instrument was constructed entirely from commercial components, including a fast-modulated UV-LED for excitation, an ICCD camera with associated control and image capture software for detection, and a pulse generator for synchronizing excitation and detection. The instrument is sensitive enough to acquire images of 200 nm, europium chelate-impregnated microspheres, or beads, by integrating 50 excitation/emission cycles during a single camera frame (66.7 ms), while completely eliminating short-lifetime fluorescence background. To assess the system's ultimate sensitivity, we imaged single, 40 nm beads that each contained approximately 400 europium chelates. The images were analyzed to determine the number of photons collected per bead, the image contrast and the SNR at different exposure times and camera gain levels. Using the method of osmotic lysis of pinocytic vesicles, we introduced a terbium complex, Lumi4-Tb®, into the cytoplasm of living Madin Darby Canine kidney (MDCKII) cells. TRL images of the terbium complex-loaded cells were acquired within acquisition times as short as 333 ms (110 excitation/emission cycles), and the effects of increased exposure time and frame summing on image contrast and SNR were quantitatively evaluated. From our data, we conclude that TRL microscopy with long-lifetime LC probes is fast and sensitive enough to obtain high quality images under the constraints imposed by working with physiologically relevant biological specimens.

Materials and Methods

All chemicals were purchased from Sigma Aldrich, Inc. (Milwaukee, WI). Lumi4-COOH was a gift from Lumiphore, Inc. (Richmond, CA). MDCKII epithelial cells were kindly provided by Dr. Jerrold R. Turner, University of Chicago. Dulbecco's modified eagle medium (DMEM), Dulbecco's phosphate buffered saline (PBS), fetal bovine serum, 0.25% trypsin/0.03% EDTA solution, and reagents for pinocytosis/osmotic lysis (Influx™ reagent, cat. no. I-14402) were purchased from Invitrogen, Inc. (Carlsbad, CA). NeutrAvidin®-labeled, 40 nm europium beads (cat. no. F20883), NeutrAvidin®-labeled, 40 nm fluorescein beads (cat. no. F8771), carboxylate-modified, 200 nm europium beads (cat. no. F20881) and NeutrAvidin®-labeled, 40 nm non-fluorescent beads (cat. no. F8772) were purchased from Invitrogen, Inc. (Carlsbad, CA). Elemental analysis was performed at Midwest Microlab, LLC (Indianapolis, IN). Biotinylated quartz coverslips were purchased from Microsurfaces, Inc. (Austin, TX). UV-Vis absorption spectra were recorded using a Cary 3000 spectrophotometer (Varian, Inc., Palo Alto, CA). Fluorescence emission spectra were recorded using a Fluorolog 3 fluorimeter (Horiba-Jobin Yvon, Inc., Edison, NJ). Time-resolved fluorescence measurements to determine luminescent lifetime were recorded using a Victor 3V plate reader (Perkin Elmer, Inc., Waltham, MA).

Spectroscopic characterization of europium beads

The europium chelate present in the commercially available beads from Invitrogen, Inc., tris(4,4,4-trifluoro-l-(2-naphthyl)-l,3-butanediono)-bathophenanthroline europium(III), was prepared using published methods.(40) Sodium Hydroxide (2.0 N, 1.5 mL) was added to a hot solution of 4,4,4 –trifluoro-1-(naphthyl)-1,3-butanedione (3 mmol) and europium chloride (1 mmol) in 25 ml ethanol and 2.5 ml H_2O. The hot solution was filtered to remove precipitated sodium chloride, and the solution was combined with a solution of bathophenanthroline (1 mmol) in 10 ml ethanol. The reaction mixture was cooled to RT and filtered, and the resulting white precipitate was washed with water and dried under vacuum. The precipitate was recrystallized in acetone/ethanol (1:1). The product was confirmed by CHN analysis (*calc.* C 61.69, H 3.53, N 2.18; *found* C 61.95, H 3.39, N 2.21), yield ~30%.

NIH-PA Author Manuscript

NIH-PA Author Manuscript

NIH-PA Author Manuscript

To estimate the number of europium chelates per bead, the extinction coefficient of the chelate (44,954 M^{-1} cm^{-1}) was calculated by measuring the absorption spectra of a 2.96μM solution of the europium chelate in toluene (λ_{max} = 350 nm, Fig. 2a). The absorbance spectrum of 40 nm-diameter europium beads suspended in glycerol (3.5×10^{12} beads/mL, ~5.8 nM) was measured with the spectrophotometer blanked with a glycerol solution containing an equivalent number of non-fluorescent, 40 nm beads.(41) From absorbance at 350 nm and the measured extinction coefficient of the chelate, the chelate concentration in the bead solution was calculated to be 2.15 μM. The average number of molecules per bead was calculated by dividing the calculated chelate concentration in the bead solution (2.15 μM) by the bead concentration (5.8 nM), yielding an average chelate load of ~370 molecules/bead (2.15 μM/5.8 nM).

For luminescent lifetime estimation, 100 μL aliquots of chelate (~20 nM in toluene) and 40 nm NeutrAvidin®-labeled europium beads (~20 nM in water) were pipetted into separate wells of a black 96-well plate. Fluorescence intensity was measured using a time-resolved fluorescence plate reader with 340 nm excitation (60 nm bandpass) and 615 nm emission (10 nm bandpass). Intensity values (100 μs integration) were measured at different time delays from 50μs to 800μs (50μs increments). Plots of intensity vs. delay time were fit to a single exponential (2 parameter) decay with KaleidaGraph v4.0, and lifetime was estimated from linear fit to the equation: $I(t) = I_0\exp(-t/\tau)$ with $R^2 > 0.99$; europium beads, 590 ± 3 μs; tris(4,4,4-trifluoro-l-(2-naphthyl)-l,3-butanediono)-bathophenanthroline europium(III) in toluene, 450 ± 3 μs. (Fig. (2b).(1)

The luminescence quantum yield (QY) of tris(4,4,4-trifluoro-l-(2-naphthyl)-l,3-butanediono)-bathophenanthroline europium(III) in toluene (QY = ~0.30) was determined by standard methods using quinine sulfate in 1 N sulfuric acid (QY = 0.546) as a reference chromophore.(42) Attempts to determine the QY of europium beads yielded inconsistent results, ranging from 0.04 to 0.15, with a mean value of 0.08 (4 measurements).

Preparation of europium bead test specimens

Beads were sonicated for 15 min. prior to dilution into H_2O for specimen preparation. An aqueous suspension was prepared that contained 40 nm, NeutrAvidin®-labeled europium beads (diluted 1:200 from stock) and 40 nm, NeutrAvidin®-labeled fluorescein beads (diluted 1:50 from stock). 10 μl of the suspension was pipetted onto the surface of a quartz coverslip modified with a polyethylene glycol-biotin surface. After 5 min. the coverslip was rinsed with water to remove any beads that were not bound through the Neutravidin®-biotin interaction. After drying with N_2, the coverslip was sealed to a quartz slide with Valap (1:1:1 Vaseline™:lanolin:paraffin).

Carboxylate-modified europium beads (200 nm diameter) were diluted 1:5000 in H_2O, and 5 μL was pipetted onto a clean quartz coverslip and allowed to dry in air. A 10μM solution of AlexaFluor™ 350 ($\lambda_{ex,\ max}$ = 343 nm, $\lambda_{em,\ max}$ = 442 nm) was prepared in water and 20 μL was pipetted onto a quartz microscope slide. The dried coverslip with the bead side facing down was placed onto the slide and sealed with Valap.

Preparation of live cell samples

Cell culture—MDCKII cells were cultured in Dulbecco's Modified Eagle Media (DMEM, Invitrogen) supplemented with 10% FBS, 2 mM L-glutamine, 100 unit/ml penicillin and 100 mg/ml of streptomycin at 37 °C and 5% CO_2. Cells were passaged using 0.25% trypsin/ 0.03% EDTA solution. To prepare samples for imaging, cells were trypsinized and reseeded at 14,000 cells/well into 8-well chambered slides and incubated at 37 °C and 5% CO_2 overnight.

NIH-PA Author Manuscript

NIH-PA Author Manuscript

NIH-PA Author Manuscript

Probe Delivery via Osmotic Lysis of Pinosomes—A 5μL aliquot of Lumi4-COOH (800μM in H_2O) was combined with ~1.2 equivalents of $TbCl_3$ (in ~1μL H_2O), vortexed for 5 min., and allowed to stand at room temperature for 30 min. This step effects chelation of terbium, rendering the probe luminescent. The metal-labeled Lumi4-Tb® solution (~6 μL) was combined with 14 μL of hypertonic growth medium (Influx™ reagent, Invitrogen, prepared according to manufacturer's instruction), yielding a final concentration of Lumi4-Tb® equaling 200 μM. MDCKII cells in a single well of an 8-well chambered slide were washed 1X with pre-warmed (37° C) PBS and 2X with pre-warmed hypertonic solution, respectively. Then, pre-warmed hypertonic solution containing Lumi4-Tb® was added, and the cells were incubated at 37 °C and 5% CO_2 for 10 min. The cells were then quickly washed 2X with hypotonic solution (Influx™ reagent, Invitrogen, prepared according to manufacturer's instruction) and allowed to incubate in hypotonic solution for exactly 2 min. at room temperature to effect lysis of pinosomes. The cells were then washed 2X with PBS, immersed in complete DMEM and incubated for ~1 h at 37 °C and 5% CO_2 before imaging.

Time-resolved luminescence microscope configuration

An epifluorescence microscope (Axiovert 200, Carl Zeiss, Inc., Thornwood, NY) was modified with the following components to enable TRL imaging: 1) a light emitting diode (LED) emitting at 365 nm (UV-LED-365, Prizmatix, Ltd., Southfield, MI); 2) delay generator (DG645, Stanford Research Systems, Inc. Sunnyvale, CA); 4) an ICCD, mounted on the side-port of the microscope, and camera controller (Mega-10EX, Stanford Photonics, Inc., Palo Alto, CA); and 5) a computer running Piper Control software (v2.4.05, Stanford Photonics, Inc.). A 100 W mercury arc lamp enables continuous wave fluorescence excitation. Filter cubes containing the appropriate excitation and emission filters and dichroics allowed for wavelength selection. Images were acquired through a 63X objective lens (EC Plan Neofluar, 63X 1.3 N.A., Carl Zeiss, Inc.).

The LED excitation source provides a collimated output that we measured to equal ~50 mW at the exit window when operated at an injection current of ~400 mA (maximum injection current is 500 mA). The LED circuitry allows for continuous wave emission or external TTL modulation with sub-microsecond rise/fall times. The excitation intensity could be varied, however, we held the intensity constant at a measured value of 1.6 mW at the objective back aperture. By taking into account the field number of the Zeiss EC Plan Neofluar objective (25 mm), its magnification (63X), and its transmittance at 365 nm (~50%, manufacturer's specifications), we estimated the illumination intensity to equal ~0.6 W/cm^2 at the image plane.(43)

The camera platform consists of an intensifier with a filmless GaAsP Extreme photocathode (Quantum Efficiency = ~0.4 from 450–600 nm, ~38% at 610 nm) fiber-optically coupled with a 1.6:1 taper ratio to a Sony XX285 CCD sensor. The CCD sensor is a 1380 × 1024 array of 6.47 μm^2 pixels, and the effective pixel size of the intensifier/camera is 10.35 μm^2. The CCD can be read out at a full-frame rate of 15 frames-per-second with a read noise of 10 electrons rms. The intensifier can be externally gated with a time resolution of 5 ns, and modulation of the multi-channel plate voltage allows for variation in gain levels to a maximum of ca. 84,000.

The delay generator mediates synchronization of the LED and the image intensifier. Piper Control software (Stanford Photonics, Inc., v2.4.05) synchronizes the camera frame clock with an external TTL pulse routed to the delay generator to begin the image acquisition sequence. The delay generator can be programmed to generate a burst of TTL output signals directed to the LED and the intensifier (routed through the camera controller). This configuration allows the user to define the LED pulse width (T) and pulse period (T′), the intensifier gate delay (Δt), the intensifier gate width (T_0), and number of excitation/emission

NIH-PA Author Manuscript

NIH-PA Author Manuscript

NIH-PA Author Manuscript

cycles that occur in a single camera frame (Fig. 1). The emission signal from multiple cycles is integrated on the CCD and read out to the image capture card of the computer at the end of the frame. The frame length can be varied as multiples of the camera frame clock, from 1 clock (66.7 ms) up to a maximum of 30 clocks (2 s). The camera control software allows for either summation or averaging of an arbitrary number of frames, and generates images in Tagged Image File (TIF) format.

Detector Calibration

For each intensifier gain level, the proportionality factor (*g*) relating image intensity values to the apparent number of photons was measured from a graph of variance versus mean intensity for a set of images. To determine variance, a pair of images of a uniform field of a luminescent sample was collected in rapid succession. A dark frame image was also captured with the LED off. The dark frame was subtracted from each of the paired images to give a new pair of images. One of these was subtracted from the other to give a difference image, leaving mainly Poisson noise with variance equal to twice the variance of a single image. Similarly, the variance was calculated for different exposure times and plotted against the mean intensity for each image pair giving a slope equal to *g*.

Data collection

For quantitative imaging of 40 nm europium beads, test specimens containing both fluorescein and europium beads were mounted on the microscope and examined through the eyepiece under continuous wave, Hg lamp excitation with a fluorescein filter set (λ_{ex} = 480/40 nm, λ_{em} = 535/50 nm). Emission from fluorescein beads was visible through the eyepiece, allowing location of the plane of focus. The larger (200 nm) europium beads were visible through the eyepiece under continuous wave excitation (λ_{ex} = 365 nm, λ_{em} = 620/20 nm), allowing focusing without co-deposition of fluorescein beads. TRL images of both 40 nm and 200 nm europium beads were captured using the 63X EC Plan Neofluar objective and the following filter set: excitation filter, G365, Carl Zeiss, Inc.; dichroic, FT395, Carl Zeiss, Inc.; narrow-pass emission filter, D620/20m, Chroma Technology Corp., Bellows Falls, VT. The emission filter effectively transmitted light from 605 nm to 630 nm with ~80% transmittance at 610 nm (the emission maximum of the europium beads used in this study).

The source and camera timing parameters that were implemented for time-resolved imaging are delineated in Table 1. For all time-resolved images, the illumination intensity at the sample plane was 0.6W/cm^2. For quantitative analysis of emission from 40 nm europium beads, multiple images of the same field of view were collected at different exposure times that were determined by setting the number of frame clocks in the camera control software. Fifty excitation/detection cycles were implemented per single frame clock of 66.7 ms duration. For example, a setting of 5 frame clocks yielded a total frame length of 333 ms during which time 250 excitation/detection cycles were implemented. Frame summing was implemented with the camera control software to acquire composite images (tagged image file format, .TIF) of 1 or 4 frames with pixel depths of 1024 (10-bit) or 4096 (12-bit), respectively. The saturation level is 16 bits (pixel depth, 65,536), achieved upon summation of 64 frames. The camera software clamps saturating signals, however, clamping was not evident at the low signal levels observed here. Series of bead images were collected at three different intensifier gain voltages: 778 V, 889 V and 944 V. By correlating these voltages against manufacturer's calibration data, the estimated gain values were 5,000, 21,900 and 45,500, respectively.

NIH-PA Author Manuscript

NIH-PA Author Manuscript

NIH-PA Author Manuscript

Image analysis

Image analysis and processing (cropping, contrast setting) was performed using NIH ImageJ (v.1.34). Further adjustment of contrast, as needed, was performed using Adobe Photoshop (v. 7.0). Image processing parameters (image size, pixel depth, min./max. gray values) are provided in Table 1.

For evaluation of 40 nm europium beads, images were analyzed visually to locate candidate single beads. As an initial filter, all bright pixel regions that appeared in sequential images were selected for analysis. Bright pixels near the edge of the field of view were excluded to minimize effects of varying illumination intensity. To distinguish between single beads and clusters of multiple beads, we measured the net integrated intensity of a 3 × 3 pixel region of interest (ROI) centered on each candidate bead in a 4-frame image collected at high gain level (944 V) with a frame length of 2 s (1500 exposures per frame, total image acquisition time = 8 s).

In order to calculate net integrated intensity, local per-pixel background (*b*) was first determined by measuring the raw intensity in a 25 × 25 pixel ROI centered on a single bright pixel region and subtracting from this the net integrated intensity in a central 3 × 3 box (Fig. 3), and *b* was given by the following equation:(39)

$$b = \frac{\sum_{-12}^{12}\sum_{-12}^{12} I_{x,y} - \sum_{-1}^{1}\sum_{-1}^{1} I_{x,y}}{616} \quad (1)$$

Pixel intensities within the 3 × 3 pixel ROI centered on the bead were summed to give the raw intensity. Net intensity (*S*) was calculated by subtracting the background in the 3 × 3 box from the raw intensity:

$$S = \sum_{-1}^{1}\sum_{-1}^{1} I_{x,y} - 9b \quad (2)$$

We then generated a histogram of net integrated intensities that revealed three regions corresponding to single beads and clusters of two or three beads. The histogram analysis revealed the location of 29 single beads within the field of view, and the ROI's containing these single beads were retained for subsequent analysis of the remaining images.

A similar histogram analysis was performed on an image of 200 nm beads to assure evenness of illumination throughout the field of view. From the histogram analysis, 25 beads were identified that were distributed evenly throughout the image, and the net integrated bead intensity was measured to be 26,600 ± 2660 (mean ± s.d.). No particular trend in measured intensity was observed in different regions of the image, indicating uniform excitation intensity across the field of view.

Images of 40 nm beads were further evaluated by calculating the net number of photons collected from each bead. Net integrated signal intensity, *S*, was divided by the appropriate camera gain factor, *g*. When appropriate, this value was divided by the number of frames summed because frame summing proportionally scales the pixel depth of the image, and net photons per bead is given by:

NIH-PA Author Manuscript

NIH-PA Author Manuscript

NIH-PA Author Manuscript

$$N = S/(g * no.frames). \quad (3)$$

Contrast (C) is defined as the magnitude of S relative to the magnitude of the expected Poisson fluctuations in background over the central 3 × 3 pixels of a bead ROI:

$$C = \frac{S}{\sqrt{9b}} \quad (4)$$

SNR was defined as the mean signal divided by the error in the signal, and mean signal was calculated as the net integrated intensity divided by the area of the central 3 × 3 pixel array. The error in the signal was taken to be the standard deviation in pixel gray value of the local 25 × 25 ROI because this gave a larger sample size than the 3 × 3 array. SNR was then calculated for each 40 nm bead in each image as:

$$SNR = \frac{S/9}{\sigma_b} \quad (5)$$

Analogous measurements (net photons, contrast, SNR) were made of images of MDCKII cells loaded with Lumi4-Tb®. The net, per-pixel emission signal intensity was calculated according to the equation: $\bar{S} = (\mu_{signal} - \mu_{bckg})$, where, μ_{signal} is equal to the mean pixel gray value in a ROI corresponding to the area of a cell, and μ_{bckg} is equal to the mean pixel gray value in a nearby ROI of equivalent area. The mean number of photons per pixel in a given cell was calculated by dividing the net intensity by the appropriate camera gain factor and number of frames: $\bar{N} = \bar{S}/(g*no.\ frames)$. Contrast was defined as the net signal intensity divided by the square root of the mean pixel gray value in the background region: $C = \bar{S}/(\mu_{bckg})^{1/2}$. For a given cell in an image, SNR was defined as the mean signal divided by the error in the signal. Because signal levels varied widely over the area of a cell (e.g., between cytoplasm and nucleus), the signal error was taken to be the standard deviation in pixel gray value for a neighboring background ROI, and $SNR = \bar{S}/\sigma_{bckg}$. The mean values of photons per pixel, contrast and SNR were reported from analysis of 6 cells in each image (Table 2).

Photobleaching analysis

To determine the photobleaching kinetics of tris(4,4,4-trifluoro-l-(2-naphthyl)-l,3-butanediono)-bathophenanthroline europium(III) in bead specimens, 200 nm europium beads were dispersed onto coverslips, mounted on the microscope and exposed to continuous wave LED illumination at the standard intensity used in this study (0.6 W/cm^2). A field of view was imaged at successive timepoints, and the net signal intensity (Equation 2) determined for 20 single beads in each successive image (see Table 1 for imaging parameters). The measured signal intensities were normalized to the initial values (t = 0), plotted against accumulated irradiation time and fit to a two-exponential (4 parameter) decay curve with KaleidaGraph v4.0: $I(t) = a*\exp(-t/\tau_1) + b*\exp(-t/\tau_2)$ (Fig. 2c). The bead luminescence decayed with a major component (71% amplitude) of 0.39 min. and a minor component (29% amplitude) of 2.88 min. R^2 residuals equaled 0.98 and showed no structure (Fig. 2c inset).

Results

The instrument's ability to suppress short-lifetime fluorescence can be clearly seen by comparing images of 200 nm europium beads acquired in continuous-wave fluorescence and

NIH-PA Author Manuscript

NIH-PA Author Manuscript

NIH-PA Author Manuscript

TRL detection modes (Fig. 4). The beads were deposited on quartz coverslips and immersed in a 10 uM solution of AlexaFluor™ 350. With continuous-wave 365 nm excitation and >420 nm long-pass emission, the europium beads were faintly visible through the eyepiece of the microscope, but the camera could not resolve the beads from background fluorescence of the dye (Fig. 4a). By imposing a time delay of only 2 μs between excitation and detection, AlexaFluor™ 350 emission was completely suppressed, and the beads were clearly visible in the TRL image (Fig. 4b). The time-resolved image (Fig. 4b) shows considerable variability in the brightness of the beads. However, a histogram analysis (see Materials and Methods, Image analysis) revealed distinct regions of intensity corresponding to single beads and clusters of 2 or more beads. The measured net signal intensities of single beads varied ~10% (26,600 ± 2660, mean ± s.d.), and this value is comparable to similar calibration beads developed for time-resolved measurements that have a coefficient of variation of 7%.(44)

TRL image acquisition parameters were optimized to collect the maximum luminescence signal under conditions of sub-saturation illumination intensity.(20,25) Thus, the excitation pulse width and the intensifier gate interval were both set to approximately equal the lifetime of the europium luminescence ($T = T_0 = 600$ μs). The output from 50 excitation pulses (pulse period, $T' = 1300$ μs) was integrated on the CCD within a single camera frame of 66.7 ms (the fastest full-frame readout speed of the camera) at a gain level of ~5,000 (778 V, see Table 1 for complete description of image acquisition and processing parameters for this and other images and data in the paper). The combination of rapid excitation/detection cycling and emission signal amplification yielded image acquisition times (66.7 ms) that were 450-fold shorter than those previously reported in a study that imaged similarly sized (107 nm) europium microspheres with a chopper-gated, cooled CCD camera at acquisition times of ~30 s.(45)

In order to evaluate the speed, sensitivity and precision of our TRL microscope at the limits of detection, we prepared a test specimen consisting of 40 nm, NeutrAvidin®-labeled europium beads deposited onto biotinylated quartz coverslips. The beads were reportedly impregnated with a luminescent europium chelate, tris(4,4,4-trifluoro-l-(2-naphthyl)-l,3-butanediono)-bathophenanthroline europium(III) (Invitrogen, Inc., personal communication). In order to confirm the identity and number of chelates per bead, we prepared the chelate and measured its excitation and emission spectra, quantum yield and luminescent lifetime, and we compared these values to measurements of the beads. The chelate and beads have identical excitation and emission spectra (Fig. 2a) and both exhibit single-exponential luminescence decay kinetics (Fig. 2b). We estimated the lifetime of the chelate in toluene to be 450μs, and the lifetime of the beads was somewhat longer (590μs), possibly due to the protective effect of the polymer matrix.(44) From absorbance measurements of the beads and a measured extinction coefficient of ~45,000 M^{-1} cm^{-1} for the chelate (at $\lambda_{em} = 350$ nm), we estimated that each bead contained, on average, 370 chelate molecules. The luminescent quantum yield of the chelate was measured to be 30% in toluene. Unfortunately, we were unable to accurately determine the quantum yield of the beads. Four separate measurements yielded values ranging from 4% to 15%, with a mean value of 8%.

To evaluate microscope performance, we adapted the methods of Murray, *et al.* to characterize bead images with respect to the number of photons acquired per bead, the image contrast, and the SNR.(39) We captured a series of images of the same field of view at different exposure times, numbers of frames and camera gain levels. The pulse/detection timing parameters were consistent for all images: excitation pulse width (T) = 600 μs; intensifier gate interval (T_0) = 600 μs; gate delay (Δt) = 10 μs; and pulse period (T') = 1300 μs. Frame length could be varied as multiples of the camera frame clock (1 clock = 66.7 ms), and 50 excitation/detection cycles were implemented per frame clock. Therefore, by

NIH-PA Author Manuscript

NIH-PA Author Manuscript

NIH-PA Author Manuscript

increasing frame length, exposure time was increased, and more signal was integrated on the CCD sensor before readout. For all measurements, the illumination intensity was held constant at approximately 0.6 W/cm^2 at the sample focal plane. Each image yielded 29 individual beads for data analysis.

Figure 5(a) shows a comparison of photon acquisition efficiency expressed as the average number of photons above the background collected from all single beads in an image as a function of exposure time for three different gain settings. For each image, four frames were summed, and a feature of the image acquisition software that removes random bright spots (saturated pixels resulting from intensifier ion-feedback noise) was implemented. Thus, frame summing had the effect of filtering extreme fluctuations in pixel intensity and reducing the overall variation in pixel background, at the expense of total image acquisition time. The net photons detected per bead was roughly the same for all gain levels within the experimental error, increased proportionally with increasing exposure time and is within the range expected considering the number of molecules per bead, the luminescent lifetime, and the likely detection efficiency of the microscope (see Discussion). The number of photons detected at the longest exposure time (0.90 s, 1500 excitation/emission cycles) was less than expected (~120 photons per bead detected; ~150 photons per bead expected) based on the observed value at 0.6 s exposure time (~100 photons, Fig. 5a). As the chelate in the beads decays bi-exponentially with a major component of the decay time equal to ~0.4 min. (Fig. 2c), the repeated exposure of the same field of view may have diminished the luminescence of the beads, as the images at long exposure times were collected last in the sequence.

In order to quantify the perceived visibility of single beads, we calculated the ratio of the above-background intensity of each bead to the size of fluctuations in a bead-sized patch of background. The visual impression of the size of a single bead seems limited to about 3 × 3 pixels (Fig. 3). This is consistent with a diffraction-limited spot of ~0.25 μm magnified 63X (~16 μm) that overfills the effective pixel size of the detector (~10 μm). Thus, we calculated contrast as $C = S/B^{1/2}$, where B is the sum of the background in a bead-sized patch (3 × 3 pixels, defined as 9b, equation 4). Figure 5(b) presents the mean contrast for all beads in a single image at each acquisition condition. Contrast appears to increase initially with the number of excitation/emission cycles, and higher gain levels yield higher contrast. While the magnitude of the contrast is somewhat arbitrary, the relative values at different gain levels correlate with the perceived visibility of beads in the images. This can be seen clearly in Figure 6, where single beads are more perceptible in the image taken at the highest gain level.

While the ability to detect weak signals increases with intensifier gain level, the precision with which faint signals can be measured is the same at all gain levels tested. Precision is indicated by the SNR, which for an image can be represented as the mean signal intensity divided by the error in the signal. Here, we calculated SNR as the net, per-pixel signal intensity from single beads, divided by the standard deviation in local pixel background gray values (equation 5). We then plotted the average value of SNR for all beads in a single image at each acquisition condition (Fig. 5c). If the major noise source in the measurements were stochastic fluctuations in the number of photons acquired per bead (Poisson noise), then the SNR should increase in proportion to $S^{1/2}$. However, we observed no increase in SNR at either longer exposure times or higher gain levels (Fig. 5c) because the noise measured was far greater than the expected contribution of Poisson noise. The observed trend in SNR is due to the fact that the image intensifier not only amplifies the signal but also adds noise. Each photon entering the image intensifier yields a burst of output photons, and the variation in the gain for each incoming photon and the correlation in time of the output photons contributes to added noise. Furthermore, the intensifier also amplifies background photons that may be present due to residual light from the excitation source,

NIH-PA Author Manuscript

NIH-PA Author Manuscript

NIH-PA Author Manuscript

phosphorescence or delayed luminescence from sample or optics, or ambient room light (see Discussion).

We next assessed the instrument's ability to capture high-resolution, time-resolved images of living cells that contained a luminescent terbium complex, Lumi4-Tb®. Lumi4-Tb® is a proprietary analog of a multidentate, 2-hydroxyisophthalamide terbium chelate previously developed by Raymond and co-workers.(46) The molecule is brightly luminescent, exhibiting characteristic terbium emission (Fig. 7a) with a quantum yield in water of 0.6 and lifetime of 2.7 ms (manufacturer's specifications). Like most LC's, Lumi4-Tb® will not passively diffuse into the interior of living cells from culture medium. Therefore, we used the method of osmotic lysis of pinocytic vesicles to effect delivery of Lumi4-Tb® to the cytosoplasm of adherent MDCKII epithelial cells. The pinocytic loading method is well established for delivering macromolecules into the cytoplasm,(47⁻48) and we have successfully adapted this method in our laboratory for LC delivery.(36) With this method, cells are allowed to undergo pinocytosis in a hypertonic medium containing sucrose, polyethylene glycol and the Lumi4-Tb®. Upon transfer to a hypotonic medium, the pinocytic vesicles burst due to the lowering of osmotic pressure, releasing their contents into the cytoplasm. The overall amount of probe molecule delivered into cells can be controlled by varying its concentration in the hypertonic loading medium, or alternatively, by repeated applications of the pinocytosis/lysis process.

Upon cellular delivery, Lumi4-Tb® appears to diffuse freely throughout the cytoplasm and nucleus without apparent non-specific binding, although some of the cells show more brightly luminescent nuclei (Fig. 7b,c). The terbium luminescence is plainly visible when only 110 excitation/emission cycles are integrated within a single camera frame of 333 ms duration (Fig. 5b, left; see Table 1 for image acquisition parameters). Image quality is improved when more excitation/emission cycles (440) are integrated during a single camera frame of 1333 ms (Fig. 5c, left). Image quality is further enhanced by summing 4 frames at either exposure level (Fig. 5b,c, right). We quantified the differences in observed image quality by calculating the number of photons per pixel, the image contrast, and SNR on a cell-by-cell basis. Increasing the number of excitation/emission cycles proportionally increases the number of photons detected per pixel and the image contrast (Table 2). Frame summing also increases image contrast, and likewise increases SNR by a factor of ~1.5 at either exposure condition (Table 2). Importantly, we visualize Lumi4-Tb luminescence in living cells at total image acquisition times ranging from 0.33 s to 5.33 s, suggesting that TRL microscopy, as we have implemented it should be useful for collecting biologically relevant data from live cell specimens (see Discussion).

Discussion

The well established benefits of TRL detection in cell-free bioassays have motivated considerable efforts to develop LCs and other long-lived probes for cellular imaging applications.(2،6،8،14،36⁻38) Underlying these efforts is an assumption that autofluorescence background elimination will considerably enhance the sensitivity of cellular imaging relative to that routinely observed with steady-state detection of short-lifetime fluorescent proteins or organic fluorophores. However, it is worthwhile to consider that live cell imaging requires adequate photon acquisition from a limited number of luminescent species. For example, over-expressed fluorescent proteins are typically imaged in mammalian cells at concentrations of 1–10 μM (ca. 10^6–10^7 copies per typical cell of 1–2 pL volume).(49) Similarly, fluorescent indicators used to image analyte concentration (e.g., Ca^{2+}, Zn^{2+}) are preferably loaded into cells at ~10–20μM concentration.(50) These cellular concentration levels reflect a need to balance detectability with minimal perturbation of physiological function. Assuming a diffuse cellular distribution, a diffraction limited volume

NIH-PA Author Manuscript

NIH-PA Author Manuscript

NIH-PA Author Manuscript

element (~1 fL) may contain <1000 fluorescent molecules. Furthermore, exposure times are limited by the need to resolve dynamic biological processes and to limit photobleaching of probes and photodamage to cells. Given these constraints, a primary motivation of this work was to explore the limits of sensitivity and time resolution that can be achieved with TRL microscopy of long-lifetime LC probes.

The number of photons detected from a single lanthanide specimen is dependent on the number of molecules in the illumination volume, the efficiency with which those molecules are excited, and the photon collection efficiency of the time-resolved detection system.(51–54) For our microscope system, the probability of exciting a single europium chelate molecule can be estimated using the following equation:(51,53)

$$E_{ex}=2.303\times 10^{3}\frac{\varepsilon\lambda_{ex}I_{ex}T}{N_{A}hc} \tag{6}$$

where, ε is the extinction coefficient of the europium chelate at the excitation wavelength (~40,000 $M^{-1}cm^{-1}$);λ_{ex} is the wavelength of excitation light (365×10^{-7} cm); I_{ex} is the intensity of illumination at the sample plane (0.6 W cm^{-2}); T is the excitation pulse width (600 μs); N_A is Avogadro's number; h is Planck's constant; and c is the speed of light. Thus, the probability that a single pulse excites a europium chelate molecule embedded in a bead is approximately 0.10.

With time-resolved detection, the width of the intensifier gate window T_0 (600 μs) after time-delay, Δt (10 μs) permits a certain proportion E_{TRL} of the decaying luminescence emission from the probe molecules to be collected as given by:(51,53)

$$E_{TRL}=e^{-\Delta t/\tau}(1-e^{-T_0/\tau}) \tag{7}$$

where τ is the luminescent lifetime of the chelate (590 μs), yielding in this case a maximum proportion of detectable luminescence equal to ~0.63. The probability that a photon absorbed by the chelate will yield a detectable emission photon is then given by:

$$E_{em}=QY*E*QE*E_{TRL} \tag{8}$$

where QY is the quantum yield of the chelate in the beads (0.08), E is the light collection efficiency of the microscope (estimated to be 15% for our system), and QE is the quantum efficiency of the intensifier at the wavelength of emission (0.38), and E_{em} equals ~2.9×10^{-3} for detecting a photon emitted from a europium bead with our TRL microscope. The expected number of photons detected from a single, 40 nm bead is then simply equal to:

$$N=n*N_{ex}*E_{ex}*E_{em} \tag{9}$$

where n is the number of europium chelates per bead (~370) and N_{ex} is the number of excitation/emission cycles implemented in a single camera exposure. For the case where N_{ex} is 500, N equals ~54, and the measured values ranged from 45 to 55 under these conditions (Fig. 5c), in excellent agreement with the calculation.

NIH-PA Author Manuscript

NIH-PA Author Manuscript

NIH-PA Author Manuscript

We evaluated performance in terms of photon detection efficiency, image contrast and SNR. The relative importance of any one of these factors will ultimately be dictated by the needs of a particular application. For example, if the goal is to detect faint signals, the best performance is achieved by operating the camera at high gain levels. However, if precise quantification of luminescence is required, no enhancement in SNR is realized by imaging at high gain or by increasing the number of excitation/emission events beyond that needed to achieve adequate image contrast. In all cases, frame summing will improve the SNR at the expense of overall image acquisition time. We observed that the SNR is lower than that expected based on the photon counts at all gain levels measured.

One factor that may contribute to sub-optimal SNR is the presence of a significant background signal that we attribute to phosphorescence from the microscope objective itself. The observed signal level was striking when we acquired TRL images of clean glass and quartz microscope slides through a long-pass emission filter ($\lambda > 420$ nm). The slide images were acquired using the same timing parameters as for the bead images, a gain level of 778 V and a single camera frame of 666 ms during which 500 excitations were implemented (10-bit image, pixel depth = 1024). The full-field, mean pixel gray values for the glass and quartz slide images were 781 and 257 respectively, with gray values approaching detector saturation level in the brightest regions of the glass slide image. The mean gray value observed without any slide or immersion oil on the objective was similar to the level observed with clean quartz slides. Much of the background signal in bead test specimens (measured on quartz substrates) was filtered out by capturing europium emission through a narrow pass filter, however a residual component was still present that added noise to the images.

While Connally and co-workers have shown that commercial UV LED's emit a weak, long-lifetime visible light signal, (30،55) we rule this out as a substantial source of non-specific background for three reasons: 1) the excitation and emission filters should effectively remove any visible component (for filter details, see Materials and Methods, Data Collection); 2) the observed signal level with no objective in the light path is negligible (i.e., effectively attenuated by the excitation filter); and 3) different objective lenses result in varying levels of observed signal. Imaging quality microscope objectives are constructed from multiple glass lenses of varying composition that are often coated with thin, anti-reflective films. Therefore, practical implementation of TRL microscopy requires careful selection of objective lenses that exhibit minimal phosphorescence.

In live-cell imaging experiments, we observed that it was possible to visualize a luminescent terbium complex, Lumi4-Tb®, diffusely distributed throughout MDCKII cells within image acquisition times as short as 333 ms. By increasing the number of excitation/emission cycles and/or summing multiple frames, the overall quality of cell images was improved (as measured by image contrast and SNR) at the expense of increased acquisition times (Fig. 7b,c; Tables 1, 2). Furthermore, we note that the cell images presented here were captured at a moderate intensifier gain voltage (778 V, gain factor = 5000); increasing the gain improves sensitivity, and thus shortens image acquisition time, at the expense of noisier images. Given a natural rate of pinocytosis of $\leq 3\times10^{-16}$ L/min. for most cell types,(48) and assuming typical cell volumes of 1–2 pL, the estimated cellular concentration of Lumi4-Tb® was ~300 nM for the experimental conditions used in this study (single loading application, 200 μM Lumi4-Tb®, 10 min. pinocytosis, see Materials and Methods). This concentration is considerably lower than the cellular concentrations of fluorescent proteins or conventional fluorophores that are typically observed in live-cell imaging experiments (~10 μM).(49⁻50)

Our results show that high resolution, quantitative TRL microscopy can be performed on a conventional epi-fluorescence microscope using commercially available light sources and

NIH-PA Author Manuscript

NIH-PA Author Manuscript

NIH-PA Author Manuscript

detectors. The system we developed can image a few hundred LC probe molecules localized to a diffraction-limited spot within ~1 s time intervals and can be used to image lanthanide luminescence in living cells at sub-micromolar cellular concentrations. While the measured performance characteristics should be adequate for a number of live cell imaging applications, even greater sensitivity and precision could be attained by using more sensitive ICCD cameras that are capable of single photon counting. Further improvements could be realized by using shorter, more intense excitation pulses (e.g., from pulsed lasers) that would saturate probe absorption and allow for more efficient photon collection, and by minimizing phosphorescence background from microscope objectives. Thus, we conclude that practical, live-cell TRL imaging is readily achievable with current optical technologies. Ongoing efforts to develop more brightly luminescent LC's, nanoparticles and other long-lifetime probes, including europium species that can be excited with visible light should lead to further improvements in detectability.(3,6–8,32,56–58) Methods to deliver such probes to the interior of living cells and target them to selected macromolecules or sub-cellular structures should benefit a variety of live-cell imaging experiments where non-specific fluorescence background is particularly problematic.(36–37)

Acknowledgments

We thank Dr. Mike Buchin (Stanford Photonics, Inc.) for valuable insights. Lumi4®-Tb is a registered trademark of Lumiphore, Inc.

Funded by:

- National Institutes of Health (R01GM081030)
- Chicago Biomedical Consortium (C-008, with support from the Searle Funds at the Chicago Community Trust)

References

1. Lakowicz, J. Principles of fluorescence spectroscopy. 3. New York: Springer; 2006.
2. Bunzli JC. Lanthanide luminescence for biomedical analyses and imaging. Chem Rev. 2010; 110(5):2729–55. [PubMed: 20151630]
3. Leif RC, Vallarino LM, Becker MC, Yang S. Increasing the luminescence of lanthanide complexes. Cytometry A. 2006; 69A(8):767–78. [PubMed: 16969794]
4. Selvin PR. Principles and biophysical applications of lanthanide-based probes. Annu Rev Biophys Biomol Struct. 2002; 31:275–302. [PubMed: 11988471]
5. Li M, Selvin PR. Luminescent polyaminocarboxylate chelates of terbium and europium: the effect of chelate structure. J Am Chem Soc. 1995; 117:8132–8138.
6. Montgomery CP, Murray BS, New EJ, Pal R, Parker D. Cell-penetrating metal complex optical probes: targeted and responsive systems based on lanthanide luminescence. Acc Chem Res. 2009; 42(7):925–37. [PubMed: 19191558]
7. Moore EG, Samuel AP, Raymond KN. From antenna to assay: lessons learned in lanthanide luminescence. Acc Chem Res. 2009; 42(4):542–52. [PubMed: 19323456]
8. Song B, Vandevyver CD, Chauvin AS, Bunzli JC. Time-resolved luminescence microscopy of bimetallic lanthanide helicates in living cells. Org Biomol Chem. 2008; 6(22):4125–33. [PubMed: 18972043]
9. Yuan J, Wang G, Majima K, Matsumoto K. Synthesis of a terbium fluorescent chelate and its application to time-resolved fluoroimmunoassay. Anal Chem. 2001; 73(8):1869–76. [PubMed: 11338604]
10. Ghose S, Trinquet E, Laget M, Bazin H, Mathis G. Rare earth cryptates for the investigation of molecular interactions in vitro and in living cells. Journal of Alloys and Compounds. 2008; 451(1–2):35–37.
11. Mathis G. Rare earth cryptates and homogeneous fluoroimmunoassays with human sera. Clin Chem. 1993; 39(9):1953–9. [PubMed: 8375081]

NIH-PA Author Manuscript

NIH-PA Author Manuscript

NIH-PA Author Manuscript

12. Prat O, Lopez E, Mathis G. Europium(III) cryptate: a fluorescent label for the detection of DNA hybrids on solid support. Anal Biochem. 1991; 195(2):283–9. [PubMed: 1750681]
13. Selvin PR, Hearst JE. Luminescence energy transfer using a terbium chelate: improvements on fluorescence energy transfer. Proc Natl Acad Sci U S A. 1994; 91(21):10024–8. [PubMed: 7937831]
14. Botchway SW, Charnley M, Haycock JW, Parker AW, Rochester DL, Weinstein JA, Williams JA. Time-resolved and two-photon emission imaging microscopy of live cells with inert platinum complexes. Proc Natl Acad Sci U S A. 2008; 105(42):16071–6. [PubMed: 18852476]
15. de Haas RR, van Gijlswijk RP, van der Tol EB, Veuskens J, van Gijssel HE, Tijdens RB, Bonnet J, Verwoerd NP, Tanke HJ. Phosphorescent platinum/palladium coproporphyrins for time-resolved luminescence microscopy. J Histochem Cytochem. 1999; 47(2):183–96. [PubMed: 9889254]
16. de Haas RR, van Gijlswijk RP, van der Tol EB, Zijlmans HJ, Bakker-Schut T, Bonnet J, Verwoerd NP, Tanke HJ. Platinum porphyrins as phosphorescent label for time-resolved microscopy. J Histochem Cytochem. 1997; 45(9):1279–92. [PubMed: 9283615]
17. Connally RE, Piper JA. Time-gated luminescence microscopy. Ann N Y Acad Sci. 2008; 1130:106–16. [PubMed: 18596339]
18. Beverloo HB, van Schadewijk A, Bonnet J, van der Geest R, Runia R, Verwoerd NP, Vrolijk J, Ploem JS, Tanke HJ. Preparation and microscopic visualization of multicolor luminescent immunophosphors. Cytometry. 1992; 13(6):561–70. [PubMed: 1451588]
19. Beverloo HB, van Schadewijk A, van Gelderen-Boele S, Tanke HJ. Inorganic phosphors as new luminescent labels for immunocytochemistry and time-resolved microscopy. Cytometry. 1990; 11(7):784–92. [PubMed: 2272243]
20. Marriott G, Clegg RM, Arndt-Jovin DJ, Jovin TM. Time resolved imaging microscopy. Phosphorescence and delayed fluorescence imaging. Biophys J. 1991; 60(6):1374–87. [PubMed: 1723311]
21. Marriott G, Heidecker M, Diamandis EP, Yan-Marriott Y. Time-resolved delayed luminescence image microscopy using an europium ion chelate complex. Biophys J. 1994; 67(3):957–65. [PubMed: 7811952]
22. Seveus L, Vaisala M, Syrjanen S, Sandberg M, Kuusisto A, Harju R, Salo J, Hemmila I, Kojola H, Soini E. Time-resolved fluorescence imaging of europium chelate label in immunohistochemistry and in situ hybridization. Cytometry. 1992; 13(4):329–38. [PubMed: 1326429]
23. Beeby A, Botchway SW, Clarkson IM, Faulkner S, Parker AW, Parker D, Williams JA. Luminescence imaging microscopy and lifetime mapping using kinetically stable lanthanide(III) complexes. J Photochem Photobiol B. 2000; 57(2–3):83–9. [PubMed: 11154087]
24. Hanaoka K, Kikuchi K, Kobayashi S, Nagano T. Time-resolved long-lived luminescence imaging method employing luminescent lanthanide probes with a new microscopy system. J Am Chem Soc. 2007; 129(44):13502–9. [PubMed: 17927176]
25. Hennink EJ, de Haas R, Verwoerd NP, Tanke HJ. Evaluation of a time-resolved fluorescence microscope using a phosphorescent Pt-porphine model system. Cytometry. 1996; 24(4):312–20. [PubMed: 8866215]
26. Law GL, Wong KL, Man CW, Wong WT, Tsao SW, Lam MH, Lam PK. Emissive terbium probe for multiphoton in vitro cell imaging. J Am Chem Soc. 2008; 130(12):3714–5. [PubMed: 18321106]
27. Phimphivong S, Kolchens S, Edmiston PL, Saavedra SS. Time-resolved, total internal reflection fluorescence microscopy of cultured cells using a Tb chelate label. Analytica Chimica Acta. 1995; 307:403–417.
28. Vereb G, Jares-Erijman E, Selvin PR, Jovin TM. Temporally and spectrally resolved imaging microscopy of lanthanide chelates. Biophys J. 1998; 74(5):2210–22. [PubMed: 9591648]
29. Verwoerd NP, Hennink EJ, Bonnet J, Van der Geest CR, Tanke HJ. Use of ferro-electric liquid crystal shutters for time-resolved fluorescence microscopy. Cytometry. 1994; 16(2):113–7. [PubMed: 7924679]
30. Connally R, Jin D, Piper J. High intensity solid-state UV source for time-gated luminescence microscopy. Cytometry A. 2006; 69(9):1020–7. [PubMed: 16888769]

NIH-PA Author Manuscript

NIH-PA Author Manuscript

NIH-PA Author Manuscript

31. Leif RC, Becker MC, Bromm A Jr, Vallarino LM, Yang S. Fluorescence resonance energy transfer enhanced luminescence (FRETEL) of Quantum Dyes®. Proc SPIE. 2006; 6092:29–41.Enderlein, GJ.; Gryczynski, ZK., editors. Ultrasensitive and Single Molecule Detection Technologies.
32. Leif RC, Vallarino LM, Becker MC, Yang S. Increasing lanthanide luminescence by use of the RETEL effect. Cytometry A. 2006; 69(8):940–6. [PubMed: 16969811]
33. Leif RC, Yang S. An analog method to produce time-gated images. Proc SPIE. 2010; 7568:75681A–75681A-9.Farkas, DL.; Nicolau, DV.; Leif, RC., editors. Imaging, Manipulation, and Analysis of Biomolecules, Cells, and Tissues VIII.
34. Mitchell AC, Wall JE, Murray JG, Morgan CG. Measurement of nanosecond time-resolved fluorescence with a directly gated interline CCD camera. J Microsc. 2002; 206(Pt 3):233–8. [PubMed: 12067368]
35. Ramshesh VK, Lemasters JJ. Pinhole shifting lifetime imaging microscopy. J Biomed Opt. 2008; 13(6):064001. [PubMed: 19123648]
36. Rajapakse HE, Gahlaut N, Mohandessi S, Yu D, Turner JR, Miller LW. Time-resolved luminescence resonance energy transfer imaging of protein-protein interactions in living cells. Proc Natl Acad Sci U S A. 2010 In Press. 10.1073/pnas.1002025107
37. Rajapakse HE, Reddy DR, Mohandessi S, Butlin NG, Miller LW. Luminescent terbium protein labels for time-resolved microscopy and screening. Angew Chem Int Ed Engl. 2009; 48(27):4990–2. [PubMed: 19492378]
38. Thibon A, Pierre VC. Principles of responsive lanthanide-based luminescent probes for cellular imaging. Anal Bioanal Chem. 2009; 394(1):107–20. [PubMed: 19283368]
39. Murray JM, Appleton PL, Swedlow JR, Waters JC. Evaluating performance in three-dimensional fluorescence microscopy. J Microsc. 2007; 228(Pt 3):390–405. [PubMed: 18045334]
40. Bauer H, Blanc J, Ross DL. Octacoordinate chelates of lanthanides. Two series of compounds. J Am Chem Soc. 1964; 86:5125–5131.
41. Wittmershaus BP, Skibicki JJ, McLafferty JB, Zhang Y, Swan S. Spectral properties of single BODIPY dyes in polystyrene microspheres and in solutions. Journal of Fluorescence. 2001; 11:119–128.
42. Demas JN, Crosby GA. The measurement of photoluminescence quantum yields. A review. J Phys Chem. 1971; 75:991–1024.
43. Grunwald D, Shenoy SM, Burke S, Singer RH. Calibrating excitation light fluxes for quantitative light microscopy in cell biology. Nat Protoc. 2008; 3(11):1809–14. [PubMed: 18974739]
44. Leif RC, Yang S, Jin D, Piper J, Vallarino LM, Williams JW, Zucker RM. Calibration beads containing luminescent lanthanide ion complexes. J Biomed Opt. 2009; 14(2):024022. [PubMed: 19405752]
45. Harma H, Soukka T, Lovgren T. Europium nanoparticles and time-resolved fluorescence for ultrasensitive detection of prostate-specific antigen. Clin Chem. 2001; 47(3):561–8. [PubMed: 11238312]
46. Petoud S, Cohen SM, Bunzli JC, Raymond KN. Stable lanthanide luminescence agents highly emissive in aqueous solution: multidentate 2-hydroxyisophthalamide complexes of Sm(3+), Eu(3+), Tb(3+), Dy(3+). J Am Chem Soc. 2003; 125(44):13324–5. [PubMed: 14583005]
47. Okada CY, Rechsteiner M. Introduction of macromolecules into cultured mammalian cells by osmotic lysis of pinocytic vesicles. Cell. 1982; 29(1):33–41. [PubMed: 6179631]
48. Rechsteiner M. Osmotic lysis of pinosomes. Methods Enzymol. 1987; 149:42–8. [PubMed: 3695968]
49. Tsien RY. The green fluorescent protein. Annu Rev Biochem. 1998; 67:509–44. [PubMed: 9759496]
50. Sala F, Hernandez-Cruz A. Calcium diffusion modeling in a spherical neuron. Relevance of buffering properties. Biophys J. 1990; 57(2):313–24. [PubMed: 2317553]
51. Condrau MA, Schwendener RA, Niederer P, Anliker M. Time-resolved flow cytometry for the measurement of lanthanide chelate fluorescence: I. Concept and theoretical evaluation. Cytometry. 1994; 16(3):187–94. [PubMed: 7924687]

NIH-PA Author Manuscript

NIH-PA Author Manuscript

NIH-PA Author Manuscript

52. Condrau MA, Schwendener RA, Zimmermann M, Muser MH, Graf U, Niederer P, Anliker M. Time-resolved flow cytometry for the measurement of lanthanide chelate fluorescence: II. Instrument design and experimental results. Cytometry. 1994; 16(3):195–205. [PubMed: 7924688]

53. Jin D, Connally R, Piper J. Practical time-gated luminescence flow cytometry. I: concepts. Cytometry A. 2007; 71(10):783–96. [PubMed: 17868087]

54. Jin D, Connally R, Piper J. Practical time-gated luminescence flow cytometry. II: experimental evaluation using UV LED excitation. Cytometry A. 2007; 71A(10):797–808. [PubMed: 17868086]

55. Jin D, Connally R, Piper J. Long-lived visible luminescence of UV LEDs and impact on LED excited time-resolved fluorescence applications. Journal of Physics D-Applied Physics. 2006; 39(3):461–465.

56. Jiang L, Wu J, Wang G, Ye Z, Zhang W, Jin D, Yuan J, Piper J. Development of a visible-light-sensitized europium complex for time-resolved fluorometric application. Anal Chem. 2010; 82(6): 2529–35. [PubMed: 20151708]

57. Wu J, Wang G, Jin D, Yuan J, Guan Y, Piper J. Luminescent europium nanoparticles with a wide excitation range from UV to visible light for biolabeling and time-gated luminescence bioimaging. Chem Commun (Camb). 2008; 3:365–7. [PubMed: 18399209]

58. Wu J, Ye ZQ, Wang GL, Jin DY, Yuan JL, YFG, Piper J. Visible-light-sensitized highly luminescent europium nanoparticles: preparation and application for time-gated luminescence bioimaging. J Mater Chem. 2009; 19(9):1258–1264.

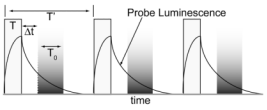

Figure 1.
Principle of time-resolved luminescence (TRL) detection. Pulsed light (width = T) excites samples. Long-lifetime probe luminescence is detected during an interval (T_0) after a short delay (Δt) allows decay of scattering and autofluorescence background. Multiple excitation/emission cycles (period = T′) can be integrated to increase signal.

NIH-PA Author Manuscript
NIH-PA Author Manuscript
NIH-PA Author Manuscript

NIH-PA Author Manuscript

NIH-PA Author Manuscript

NIH-PA Author Manuscript

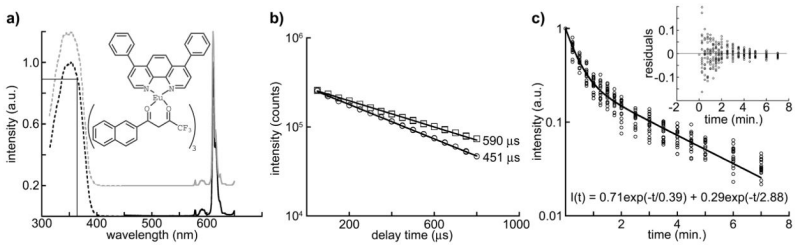

Figure 2.

Spectra, luminescent lifetime, and photobleaching kinetics of europium microspheres used in this study. **(a)** Normalized excitation (dotted) and emission spectra (solid) of 40 nm, NeutrAvidin®-labeled europium microspheres (Fluospheres™, cat. no. F20883, Invitrogen, Inc.) in water (black) and the europium chelate present in the microspheres, tris(4,4,4-trifluoro-l-(2-naphthyl)-l,3-butanediono)-bathophenanthroline europium(III) (structure, inset), dissolved in toluene (gray). The chelate spectra are shown offset for clarity. The absorbance of the beads/chelate is ~90% of maximum at the UV LED emission wavelength (365 nm), as indicated by the lines drawn on the graph. **(b)** Semi-log plot of intensity vs. delay time for 40 nm europium beads in water (squares) and europium chelate in toluene (circles). The solid lines represent single exponential (2 parameter) fits to the data, $I(t) = I_0 \exp(-t/\tau)$. The calculated lifetime is shown adjacent to the plotted curves, and three repetitions of the experiment yielded values that agreed within <4 percent. R^2 residuals were greater than 0.99 in all cases. (**c**) Semi-log plot of luminescence intensity (normalized to initial value at t = 0) vs. accumulated irradiation time for 200 nm europium beads. A field of view was exposed to continuous wave LED excitation at the standard illumination intensity (~0.6 W/cm^2), imaged at successive timepoints, and the net signal intensity determined for 20 single beads at each timepoint. The solid line is a 2-exponential (4 parameter) fit to the data: $I(t) = a*\exp(-t/\tau_1) + b*\exp(-t/\tau_2)$. The bead luminescence decayed with a major component (71% amplitude) of 0.39 min. and a minor component (29% amplitude) of 2.88 min. R^2 residuals equaled 0.98 and showed no structure (inset). Specific imaging parameters are provided in Table 1.

NIH-PA Author Manuscript

NIH-PA Author Manuscript

NIH-PA Author Manuscript

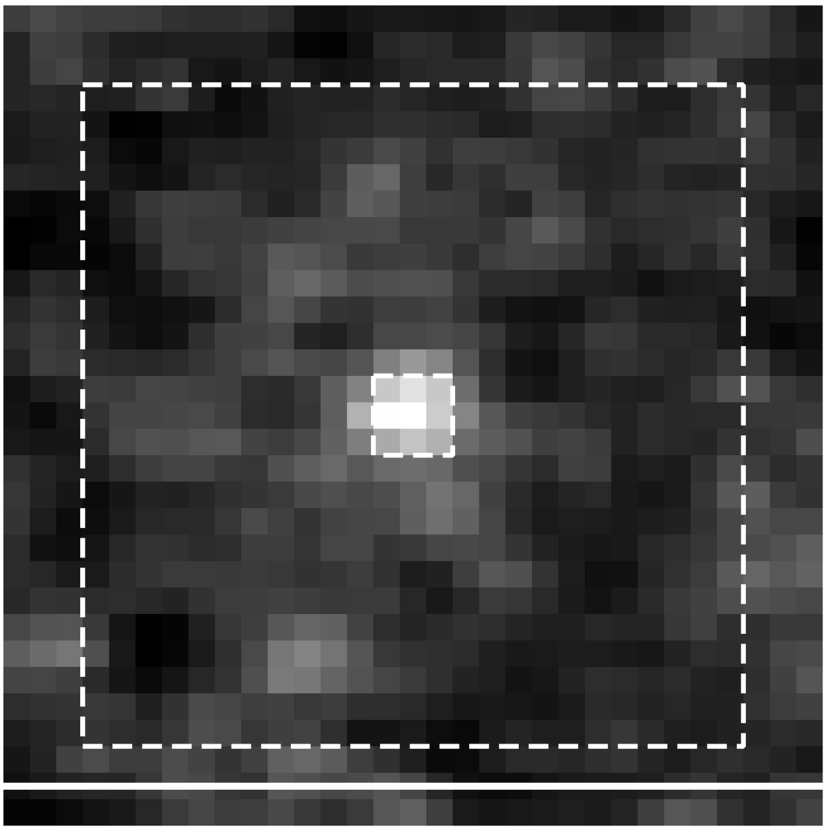

Figure 3.
Schematic of the measurement regions described in the text. The micrograph shows a region of a time-resolved image containing a single, 40 nm europium chelate-impregnated polystyrene bead. Dashed lines denote pixel array boundaries. *Raw bead intensity* is defined as the sum of the pixel values in the central 3 × 3 box. The local per-pixel *background* (*b*) is measured in a 25 × 25 pixel neighborhood that excludes the central 3 × 3 box. *Net integrated bead intensity* (*S*) is calculated by subtracting the background in the 3 × 3 box (i.e. 9*b*) from the *raw bead intensity*. TRL imaging parameters for all images and data are described in Materials and Methods and Table 1. Scale bar, 10 μm.

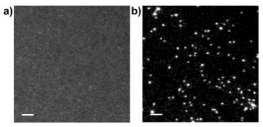

Figure 4.

Time-resolved luminescence (TRL) detection eliminates short-lifetime fluorescence background signals. Europium beads (200 nm diameter) were deposited on a quartz coverslip and immersed in a 10 μM solution of AlexaFluor™ 350. The specimen was excited with 365 nm light and emission was viewed through a long-pass (>420 nm) filter. **(a)** In continuous wave, epifluorescence detection mode, the beads cannot be resolved from the fluorescent background. **(b)** In TRL mode, a short gate delay (Δt = 2 μs) between excitation and detection eliminates background and allows clear visualization of single beads (see Materials and Methods and Table 1 for complete image acquisition parameters). Scale bars, 10 μm.

NIH-PA Author Manuscript NIH-PA Author Manuscript NIH-PA Author Manuscript

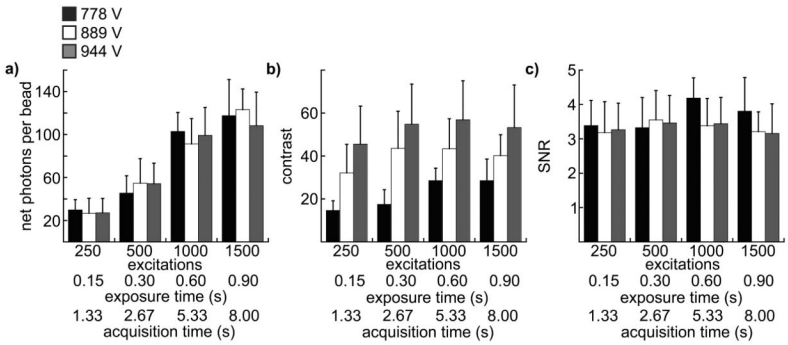

Figure 5.

Results of image analyses to determine photon acquisition efficiency, image contrast and instrument precision (SNR). Each chart presents data from 12 individual images collected at 4 different numbers of excitation/emission cycles, exposure times and total acquisition times (indicated on the x-axes) and 3 different intensifier gain voltages: 778 V (black columns), 889 V (white columns), 944 V (gray columns). Column height represents the mean value of each parameter (indicated on the y-axes) calculated from 29 single beads in a single image, and the error bars represent standard deviation. Source/detector timing parameters and frame summation (4 frames summed) were consistent for all images as described in Materials and Methods and Table 1. (**a**) The net number of photons acquired from a single bead. (**b**) Contrast. (**c**) SNR.

NIH-PA Author Manuscript NIH-PA Author Manuscript NIH-PA Author Manuscript

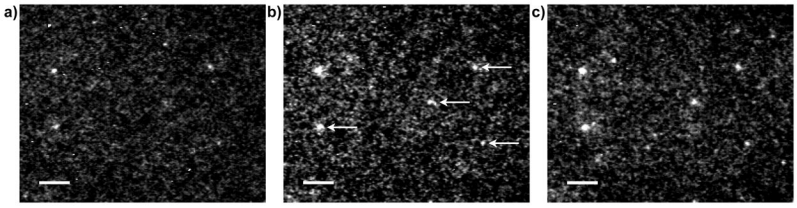

Figure 6.

Image contrast increases with intensifier gain level. Images of 40 nm europium beads acquired with 500 excitation/emission cycles and at gain levels of (**a**) 778 V); (**b**) 889 V; and (**c**) 944 V (see Table 1 for complete image acquisition and processing parameters). The arrows in image (**b**) indicate the location of single beads as verified by histogram analysis and consistent appearance in sequential images (see Materials and Methods, Image Analysis). Other bright spots in the images are either bead clusters or noise artifacts. Scale bars, 10 μm.

NIH-PA Author Manuscript
NIH-PA Author Manuscript
NIH-PA Author Manuscript

NIH-PA Author Manuscript

NIH-PA Author Manuscript

NIH-PA Author Manuscript

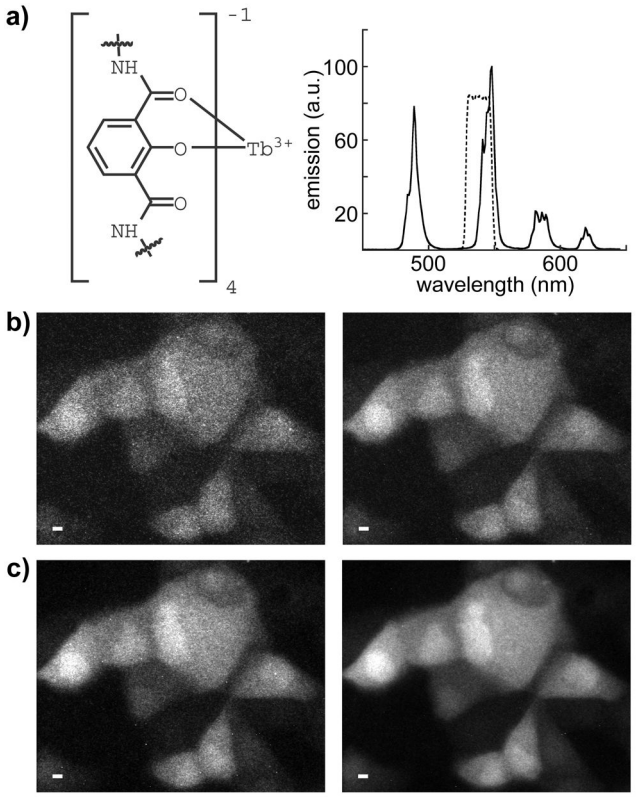

Figure 7.

Visualization of a luminescent terbium complex in living cells with time-resolved microscopy. Image quality is enhanced by increasing exposure time and summing multiple frames to generate a single image. **a) left,** partial structural representation of Lumi4-Tb®, a proprietary analog of a multidentate, 2-hydroxyisophthalamide terbium chelate reported by Raymond and co-workers;(42) **right,** characteristic terbium emission spectrum of Lumi4-Tb®. The compound emits with a quantum yield of ~0.6 and a lifetime of ~2.7 ms. A narrow-pass filter (transmittance shown as dotted lines) captures ~35% of the total terbium emission. **b–c)** Time-resolved luminescence micrographs showing MDCKII cells that were loaded with Lumi4-Tb® by osmotic lysis of pinocytic vesicles (see Materials and Methods). Complete details of data collection and image processing parameters are provided in Table 1. Scale bars, 10 μm. **b)** Images of 110 excitation/emission cycles (exposure time = 165 ms). **left,** single frame; **right**, 4 frames summed. **c)** Images of 440 excitation/emission cycles (exposure time = 660 ms). **left**, single frame; **right**, 4 frames summed.

NIH-PA Author Manuscript NIH-PA Author Manuscript NIH-PA Author Manuscript

Table 1

Summary of detection and image processing parameters for time-resolved images and data presented in the paper.

image or data	λ_{em} (nm)	excitation pulse width (ms)	gate delay (ms)	intensifier gate width (ms)	excitation events	frame length (ms)	frames summed	exposure time[b] (ms)	acquisition time (ms)	intensifier gain (V)	pixel dimensions	pixel depth	contrast (min./max.)
Fig. 2c	605–630	0.600	0.010	0.600	50	66.7	4	30	66.7	778	N/A	N/A	N/A
Fig. 3	605–630	0.600	0.010	0.600	250	333	4	150	1333	944	31×31	4096	585/1772
Fig. 4b	605–630	0.600	0.002	0.600	50	66.7	1	30	66.7	778	300×300	1024	56/1019[c]
Fig. 5	605–630	0.600	0.010	0.600	*a*	*a*	4	*a*	*a*	*a*	N/A	N/A	N/A
Fig. 6a	605–630	0.600	0.010	0.600	500	667	4	300	2667	778	250×200	4096	160/834[c]
Fig. 6b	605–630	0.600	0.010	0.600	500	667	4	300	2667	889	250×200	4096	268/1739[c]
Fig. 6c	605–630	0.600	0.010	0.600	500	667	4	300	2667	944	250×200	4096	440/2417[c]
Fig. 7b, left	530–550	1.500	0.010	1.390	110	333	1	165	333	778	900×725	1024	23/162
Fig. 7b, right	530–550	1.500	0.010	1.390	110	333	4	165	1333	778	900×725	4096	109/515
Fig. 7c, left	530–550	1.500	0.010	1.390	440	1333	1	660	1333	778	900×725	1024	31/486
Fig. 7c, right	530–550	1.500	0.010	1.390	440	1333	4	660	5333	778	900×725	4096	137/1851

[a] The data presented in Fig. 5 were acquired at varying numbers of excitations and gain levels as indicated in the text and figure legend.

[b] Exposure time indicates the total irradiation time of the sample during a single exposure. Frame summing multiplies exposure time accordingly.

[c] Contrast was adjusted to the indicated minimum/maximum pixel gray values using NIH ImageJ and further enhanced for visual clarity using Adobe Photoshop.

NIH-PA Author Manuscript

NIH-PA Author Manuscript

NIH-PA Author Manuscript

Table 2

Summary of quantitative analyses of cell images shown in Figure 7.[a]

image	photons per pixel	contrast	SNR
Fig. 7b, left	10.1/0.8	8.2/0.7	1.9/0.15
Fig. 7b, right	8.4/0.7	13.9/1.2	2.9/0.22
Fig. 7c, left	44.3/3.8	30.0/2.5	4.0/0.45
Fig. 7c, right	41.6/3.6	58.0/4.9	6.2/0.81

[a]Data are presented as mean ± s.e.m. for each value, calculated as described in Materials and Methods from 6 cells in each image. Data collection and image processing parameters are given in Table 1.